J. Earth Syst. Sci. (2019)128 213
https://doi.org/10.1007/s12040-019-1235-1

Grain-scale anatomy of the Bundelkhand granite: Implications for the interplay of magmatic to sub-magmatic deformation mechanisms

Goutam Sarkar[1], Shriza Acharya[1], Sayandeep Banerjee[1,*], Abdul Matin[2], Sarajit Sensarma[3] and Hari B Srivastava[1]

[1]*Centre of Advanced Study in Geology, Banaras Hindu University, Varanasi 221 005, India.*
[2]*Department of Geology, University of Calcutta, Kolkata 700 019, India.*
[3]*Centre of Advanced Study in Geology, University of Lucknow, Lucknow 226 007, India.*
**Corresponding author. e-mail: sayandeep87.geo@bhu.ac.in*

MS received 22 January 2019; revised 26 April 2019; accepted 16 May 2019

Grain-scale structures of the granitoid rocks from the north-western part of the Bundelkhand craton, central India are analysed with the aid of an optical microscope and electron probe micro analyser. Although field-based studies and quick microscopic observations suggest an overall porphyritic texture of the Bundelkhand granitoid, detailed microstructural observations reveal a significant deviation from the first-order igneous porphyritic texture. Here, we show that the Bundelkhand granitoid has three distinct grain-scale structures: (i) original pristine igneous structures, (ii) ductile deformation-related structures, and (iii) brittle fracturing-related structures. Based on microstructural evidences, we argue that the deformation-induced structures (both brittle and ductile) are not restricted to solid state, rather these structures initiated in the sub-magmatic stage and nucleated in partially crystallised magma during the magmatic to sub-magmatic event of the crystallisation history.

Keywords. Magmatic deformation; tectonics; microstructure; granite; Bundelkhand craton.

1. Introduction

Deformation of partially crystallised granitoid magmas, as evident from the structures observable at all scales, is fundamental in understanding the rheology, magma movement, emplacement mechanisms, ambient tectonic stress conditions and associated processes operating within the magma chamber (Fernández and Castro 1999; Barros *et al.* 2001). Most of the field-based studies (e.g., Hibbard 1987; Vernon *et al.* 2004) and laboratory experiments (e.g., Dell'Angelo and Tullis 1988; Rutter and Neumann 1995) envisaged that a range of deformational processes can be operational during the deformation of partially crystallised magma. These include suspension-type flow, grain-type flow, contact melting, expulsion of melt by filter pressing, nucleation of microscale shear zone and crystal plasticity (Park and Means 1996). The deformation of the felsic magma during crystallisation progresses in two stages. At an early stage with low crystal fractions (∼20%), the crystals independently rotate which eventually results in a magmatic fabric, while at the later stage with higher crystal fractions (>55%), the crystals start to interact among themselves, which causes strain localisation within the early formed crystals (Vigneresse and Tikoff 1999). Our ongoing

Published online: 27 July 2019

research on the granitoid rocks from the Bundelkhand craton (BC) of north-central India clearly depicts the presence of a wide spectrum of microstructures in Bundelkhand granitoid (BG) which includes pristine magmatic microstructures, ductile deformation-related microstructures and brittle fracturing-related microstructures. Here, we explore the grain-scale characteristics of the BG (both pristine and deformation-related structures) from the north-western part of the BC, that suffice for the timing of the formation of magmatic to submagmatic deformation microstructures with respect to the magmatic history of the BG.

2. Geological setting

The BC, covering an area of ∼26,000 km^2 in north central peninsular India (figure 1a) comprises the early Archaean Bundelkhand gneissic complex, metasedimentary and metavolcanics, Madawara igneous complex and Neoarchaean–Palaeoproterozoic BGs that occupy >90% of the craton (Basu 1986, 2007; Mohan *et al.* 2012). Satellite imageries clearly depict that the entire craton is dissected by E–W, NE–SW, NW–SE and N–S trending shear fractures/joints (Basu 2007). Based on the U–Pb single zircon method and the Hf-isotopic study, in consensus with the earlier results on the crystallisation age of BGs (e.g., Mondal *et al.* 2002), Kaur *et al.* (2016) suggested a crystallisation history between 2.58 and 2.50 Ga. The BGs are thought to be emplaced in a subduction-related geodynamic regime (Rahman and Zainuddin 1993; Mondal and Zainuddin 1996). The BG is intruded by NE–SW trending intrusive giant quartz reefs of kilometre-scale long and tens of metres wide and the extensive ∼NW–SE trending dolerite dyke swarms along with less abundant dykes in other orientations (Pati *et al.* 2008; Mohan *et al.* 2012; Bhattacharya and Singh 2013). The BC was affected by metamorphic events at ∼3.2 Ga (Kaur *et al.* 2016) and 2.78 Ga (Saha *et al.* 2011), followed by a 0.5–0.6 Ga pan-African tectono-thermal event (Kaur *et al.* 2016).

3. General characters of the BG

The area of study, located at the north-western part of the BC, comprises the BG rocks, which are exposed as either isolated small hillocks or flat grounds. On an outcrop scale, granitic rocks are coarse grained (figure 1b), with an overall porphyritic texture, where phenocrysts and megacrysts of alkali and plagioclase feldspar crystals are mounded in a groundmass of quartz, small-sized feldspars and amphibole. Previous workers commonly named the granitoid rocks based on their colour of hand specimens. Based on the colour of hand specimens, two end members viz., red and grey granitoid can be identified along with a

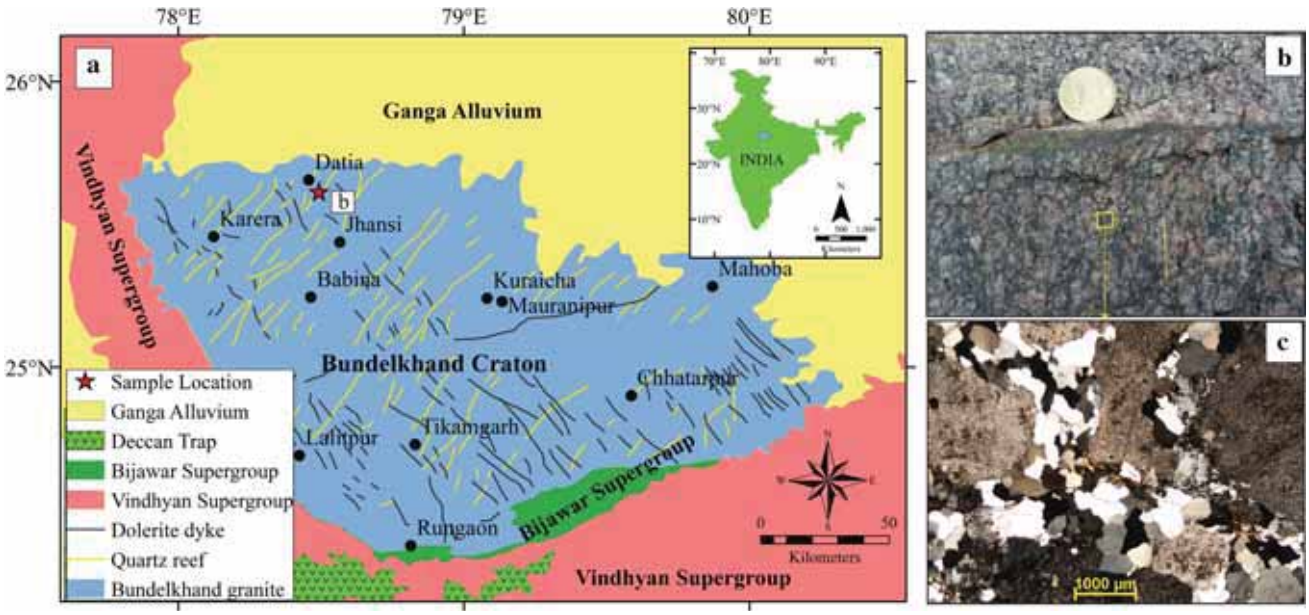

Figure 1. (**a**) Generalised map of the BC and its surrounding terrains of the north-central peninsular India (modified after Kaur *et al.* 2016). Location of the BC in India (inset). (**b**) Field photograph of the BG showing a crude magmatic fabric (dashed line). (**c**) Photomicrograph of the BG showing the undoubtedly porphyritic texture.

transitional type. The boundary between red and grey granitoid is gradational where the red-coloured granitoid fades gradually into grey-coloured granitoid with progressive decrease in red colouration. Instead of considering the red and grey granitoids are of separate entities, Sensarma *et al.* (2018) suggested that the original grey-coloured granitoid transformed to red-coloured granitoid due to mantle-derived high temperature fluid–rock metasomatic alteration. The conclusion of Sensarma *et al.* (2018) is further supported by the observation that both grey- and red-coloured granitoids show similar modal mineralogical compositions (Sarkar *et al.* 2017) and contemporaneous crystallisation age (Kaur *et al.* 2016). We, therefore, use the common term granitoid to refer to both red- and grey-coloured granitoid rocks that exhibit an undoubtedly porphyritic texture under the microscope (figure 1c). On an outcrop- to the microscopic scale, the phenocrysts and megacrysts of both feldspar crystals of the granitoid rocks are inequidimensional, elongate in shape and their long dimension often preferentially aligned to define a crude but observable foliation, which in turn shows an apparent gneissic look in the granitoid (figure 1b). The shape preferred foliation within the granitoid rocks in the area of study represents a primary magmatic fabric, the detail characters of the fabric can be found in Sarkar *et al.* (2017). The granitoid rocks with primary fabric are traversed by prominent three sets of brittle fractures and associated discrete ductile shear zones. The fractures and associated ductile shear zones are broadly oriented along ∼E–W, ∼NE–SW and ∼NW–SE (Basu 2007; Sarkar *et al.* 2017). The relationship between the fracture systems and the ductile shear zones are not discussed here and will be highlighted in a separate contribution.

4. Micro-scale structure

Microscopic analyses were performed at the Image Analyser Laboratory of University of Calcutta, Kolkata, from 26 thin sections using an advanced polarising microscope (Nikkon Eclipse Lv 100 Pol). Two thin sections, selected after a microscopic study, were further studied using a CAMECA SXFive electron microprobe analyser (EPMA) at the Department of Geology, Banaras Hindu University, Varanasi. Wavelength-dispersive spectrometry and a LaB6 source were deployed for X-ray element 'dot' mapping. For X-ray 'dot' mapping, an acceleration voltage of 15 kV and beam current of 40 nA were used, whereas 15 kV and 13 nA were deployed for back-scattered electron (BSE) imaging. The granitoid rocks have an assemblage, in order of decreasing abundance, of alkali feldspar + plagioclase feldspar + quartz with ± biotite ± amphibole ± magnetite and show a porphyritic texture in the first order. Large alkali feldspar, plagioclase feldspar and occasional amphibole crystals constitute the phenocrysts while quartz, smaller alkali feldspar, plagioclase feldspar and biotite make up the groundmass. The inequidimensional elongate phenocrysts are often preferentially aligned, with their long dimension are parallel to sub-parallel, to define a magmatic foliation which is in consistency with the outcrop- to hand sample-scale observation. All of the phases are affected by brittle fractures. Although the granitoid rocks seem to have a first-order porphyritic texture affected by brittle fractures, microscopic observations reveal a substantial deviation from the situation of ideal porphyritic texture overprinted by brittle fractures. Here, we present the detail microscopic characters of these deviations in BG from the north-western part of the BC.

The constituent minerals show three distinct grain size distributions (figure 2). First, feldspars (both alkali and plagioclase feldspar), with subordinate biotite and amphibole crystals constitute ∼50% by volume of the total rock in the form of phenocrysts and often form a framework of grains with interstitial spaces filled up by groundmass of quartz + biotite + alkali and plagioclase feldspar (figure 2a and b). Individual phenocrysts range in size from 4942 to 534 μm with an average grain size of ∼1800 μm (figure 2c and d). Second, aggregate of quartz, feldspar and biotite that constitute the groundmass, having individual grain size ranging from 498 to 61 μm and average grain size of ∼200 μm (figure 2c and e). Third, a curvilinear to an often anastomosing network of intragranular fractures confined or associated with the phenocrysts is filled with very fine-grained aggregate of quartz and feldspar. The fracture fill materials range in size from 50 to 6 μm with an average grain size of ∼20 μm (figure 2c and f). The microstructural observations reveal that each grain size class exhibits distinct microstructural characteristics. Thus, the grain-scale anatomy of phenocrysts, groundmass and fracture fills are described in detail. Phenocrysts of feldspars show the pristine magmatic structures such as the tartan twinning, albitic twinning, perthitic intergrowth structures. Partial replacement

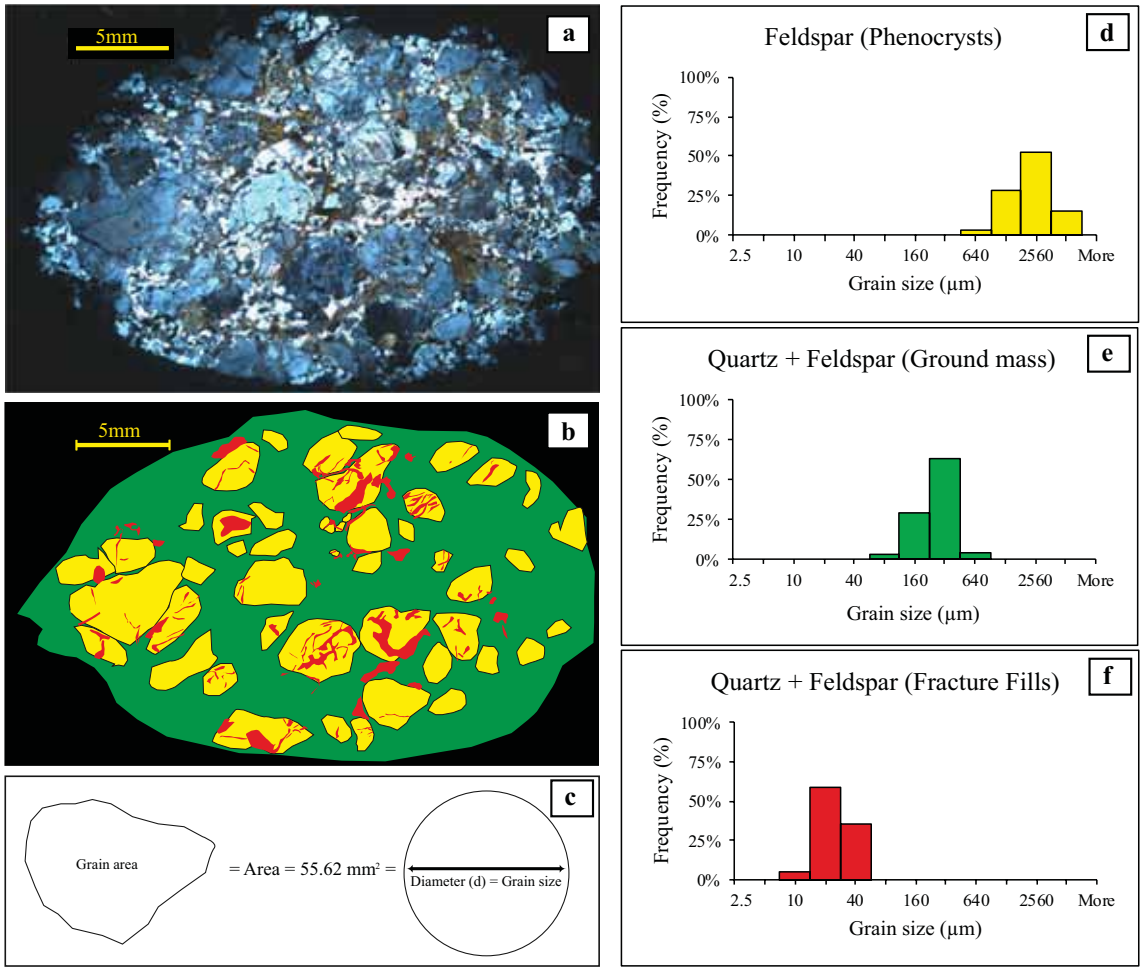

Figure 2. (**a**) Photomicrograph of the heterogeneously deformed BG. (**b**) Schematic diagram of the overall microstructure drawn from (a) showing variation in grain size. Yellow: phenocrysts; green: groundmass and red: fine-grained fracture infills. (**c**) Grain size is calculated as the diameter of the equivalent area circle. Frequency of grain size distribution of (**d**) phenocrysts, (**e**) groundmass, and (**f**) fracture infills (x-axis in the GP series, scale factor 2).

by myrmekite of K-feldspar along the contact with plagioclase is also common (figure 3a). Phenocrysts of both biotite and amphibole crystals are euhedral in outline and appear to represent the pristine magmatic structure. All of the phenocrysts bear imprints of both brittle and ductile intracrystalline deformation microstructures. The ductile intracrystalline deformation in alkali and plagioclase feldspar grains is marked by undulose extinction, deformation twinning and bending of albitic twin lamellae. The brittle intracrystalline deformation in feldspars phenocrysts are marked by intragranular and transgranular fractures, where intragranular fractures are commonly healed by fine-grained mass (figures 2 and 3b). Biotite phenocrysts show variable amounts of intracrystalline deformation and seem to be more deformed than the other phenocryst minerals. Some grains appear to be devoid of any intracrystalline deformation, whereas others show strong undulose extinction, bending and grain-scale kinking (figure 3c). Axial traces of the kinks are often fractured by intragranular fractures and often healed by fine-grained mass (figure 3d). Amphibole phenocrysts are mostly deformed by fracturing and are also filled up by very fine-grained mass. Individual grains in the groundmass are subhedral to anhedral in outline with a more or less equidimensional shape and equigranular in size, and the boundaries of the quartz grains often form triple junction with 120° angular relations. In contrast to the phenocrysts, the groundmass lacks any significant ductile intracrystalline deformation structures (figure 3e). A few quartz grains in the groundmass, however, show mild ductile intracrystalline deformation like sweeping undulose extinction and sub-grain formation (figure 3f). Transgranular fractures commonly cut across the groundmass

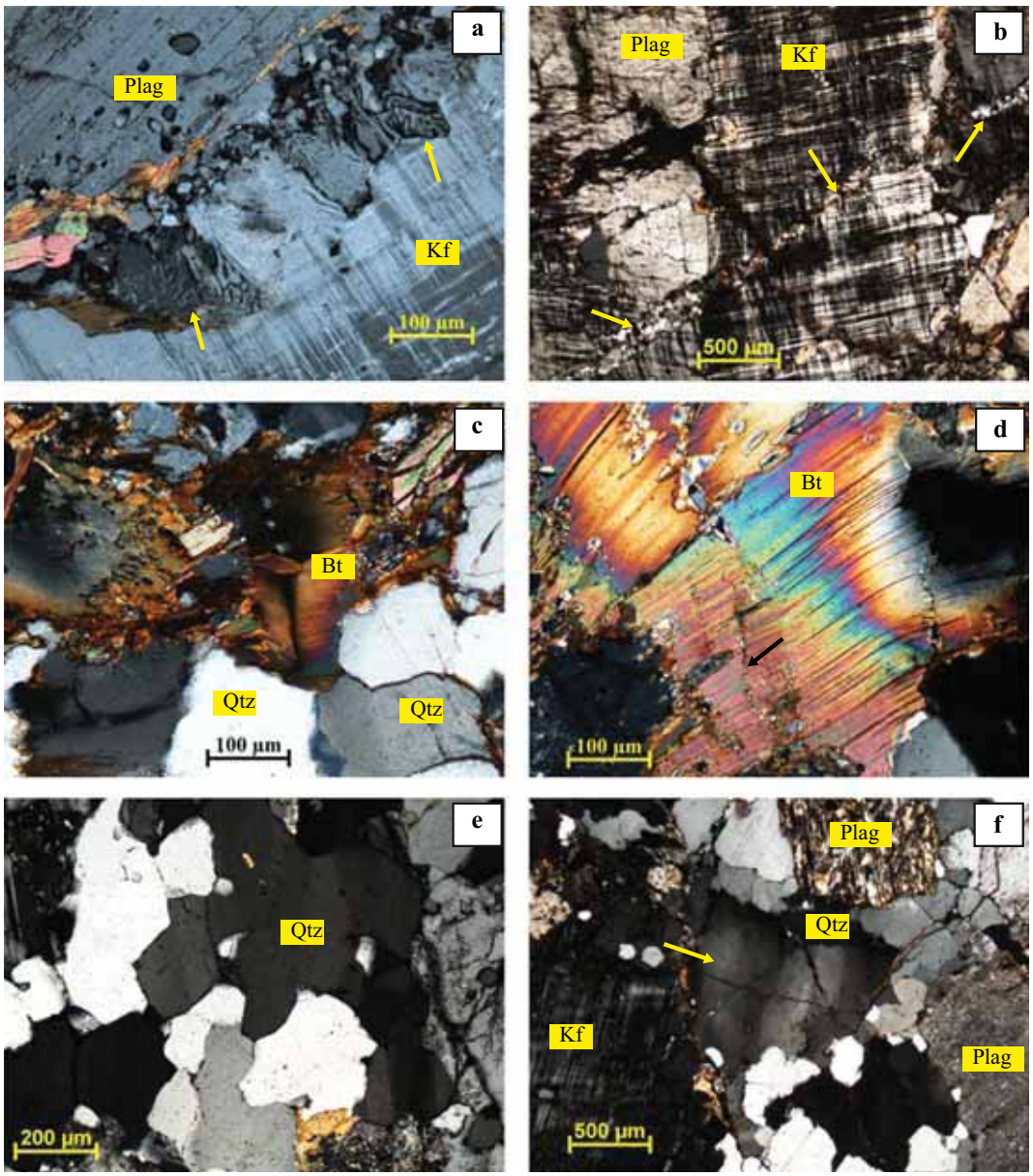

Figure 3. Photomicrographs showing the microstructural characteristics of the BG: (**a**) myrmekitic intergrowth at the contact surface of potash and sodic feldspar grains, (**b**) fracturing in feldspar, healed by fine-grained quartz–feldspar mass. Note that the fracture fill material is devoid of any intracrystalline deformation, (**c**) kinked biotite with strong intra-crystalline deformation, (**d**) kinked biotite with axial planar fracturing, healed by fine-grained mass (arrow), (**e**) deformation-free aggregate of quartz crystals occupying the interstitial spaces formed by the network of feldspar grains, and (**f**) quartz crystal showing sub-grain formation. Plag: plagioclase; Kf: potassium feldspar; Bt: biotite; Qtz: quartz.

materials, but no healing material is observed within these fractures (figure 3e). Except significantly smaller grain size, the healing mass within the intragranular fractures of the phenocrysts show more or less similar mineralogical composition like that of the groundmass. The grains in the fractures are too fine-grained to be identified with a high degree of confidence using an optical microscope. To identify the constituent minerals within the fractures in the biotite phenocrysts, X-ray maps were prepared. X-ray maps clearly illustrate that the fracture within the biotite is dominantly filled up with quartz with a minor amount of potash feldspar (figure 4).

5. Discussion

In this present study, we analysed grain-scale structures in the BG rocks from the northern part of the BC. Results of the detailed microstructural study reveal that constituent minerals of the

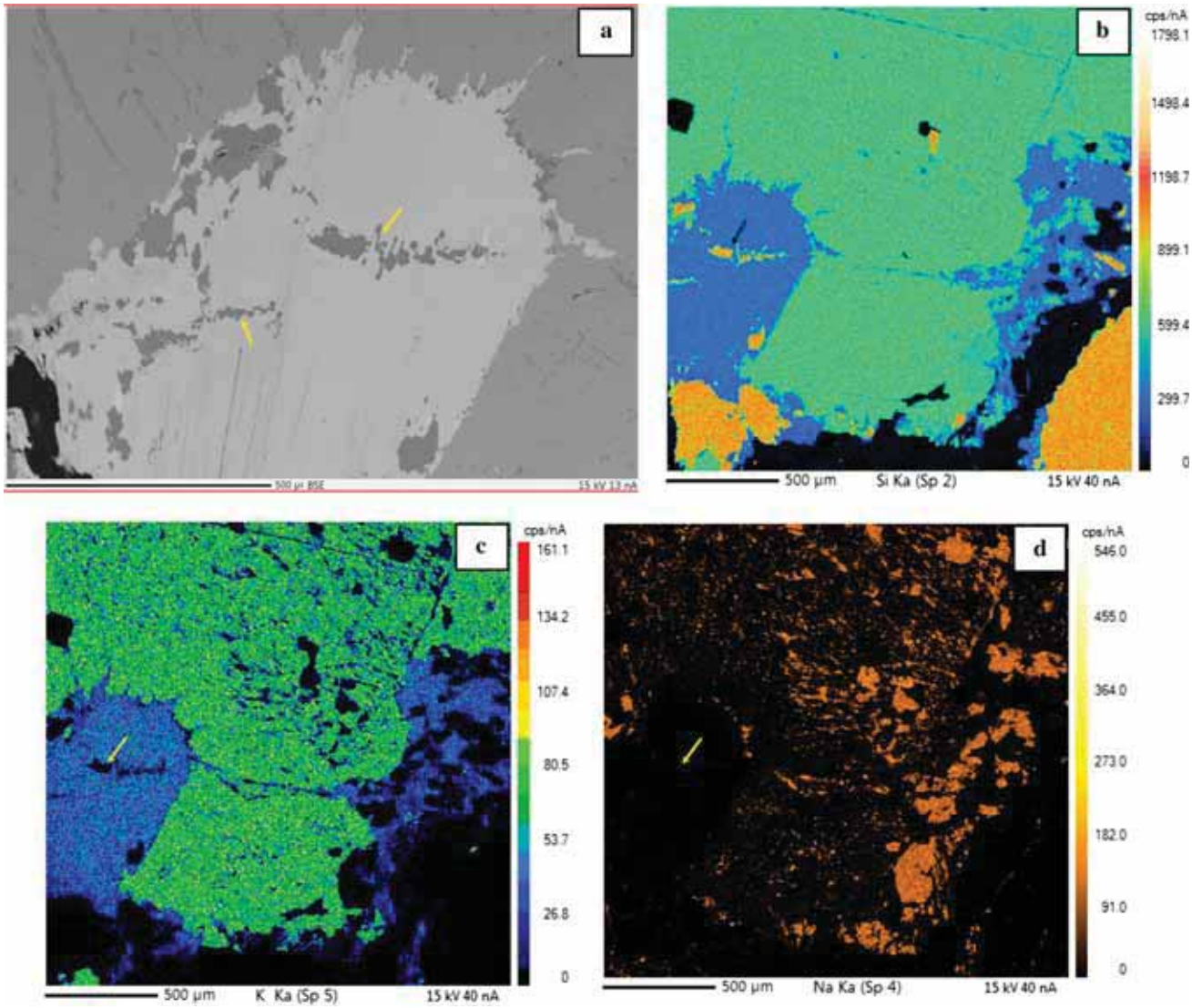

Figure 4. (**a**) BSE image of biotite with healed fracturing (arrow). X-ray (**b**) Si, (**c**) K, and (**d**) Na elemental map of the fracture fill material within biotite (arrow). X-ray maps showing (b) higher Si concentrations of the healed material compared to host biotite, (c) minute K concentration of the healed material compared to host biotite, and (d) negligible Na concentration of the healed material.

granitoid have three distinct grain-scale characteristics, viz., (i) pristine igneous microstructures, (ii) grain-scale ductile deformation structures, and (iii) brittle fracturing-related structures.

The occurrence of pristine igneous microstructures, as evidenced by the tartan twinning in microcline, albitic twinning in plagioclase, perthitic intergrowth structures and overall first-order porphyritic texture is expected to be the result of slow cooling granitoid magma (including the sub-solidus cooling) in a plutonic environment.

The presence of deformation twinning in feldspar, kinking and bending of biotite grains, undulose extinction and sub-grain formation in quartz suffice for the localised ductile deformation structures in the study area and indicate a deformation in the dislocation creep regime. The signature of melt-assisted diffusion creep, as evidenced by the myrmekitic intergrowth along the boundary of the potash feldspar phenocryst, is also noted (Dell'Angelo *et al.* 1987). However, no transposition of diffusion creep microstructures by dislocation creep microstructures is noted. These ductile deformation structures are strongly decoupled in the constituent phases and are restricted either along the grain boundary or within the large phenocrysts, while the groundmass, especially, quartz lacks any significant ductile deformation structures. The decoupling of deformation among large- and small-sized grains (phenocryst and

groundmass) is linked to the strain partitioning during the magmatic stage to sub-magmatic stage. In the magmatic stage, while the early crystallised grains or the phenocrysts were strained and preserved the evidence of solid-state deformation, the groundmass remained molten and hence escaped the solid-state deformation processes (Sarkar *et al.* 2017). At few places, however, groundmass shows mild solid-state deformation as evidenced by mild undulose extinction and sub-grain formation which may have resulted from the solidified melt pockets trapped in between phenocrysts.

Micro-scale fractures are the most commonly occurring deformational structures in the BG. The configuration of fractures varies from planar to curvy-planar and can be categorised under (a) intragranular fractures, affecting mostly feldspar, biotite and amphibole phenocrysts, which are healed by fine-grained materials with composition more or less similar to that of groundmass, while (b) transgranular fractures, affecting both phenocrysts and groundmass, are mostly devoid of any healing materials.

The healed fractures restricted within the phenocrysts are interpreted to be nucleated in the early formed crystal mush under the magmatic condition during which a substantial amount of melt had been present in the interstitial spaces between the crystals (Bouchez *et al.* 1992). The interstitial melt, now represented by the groundmass, percolates through the fractures. This hypothesis is apparently supported by these observations: (i) both the groundmass and the fracture infill lack any intracrystalline deformation in comparison with the phenocrysts; (ii) both the groundmass and fracture infill exhibit similar modal mineralogical abundances, (iii) the absence of the fine-grained fracture infills within the groundmass, and (iv) the optical continuity of the groundmass and the fracture infill materials. The grain size is, however, significantly different for the groundmass and the fracture infills. This may be related to the lack of space created by the opening of the fractures. Fracturing of early formed crystals and subsequent healing in a granitic magma, a common phenomenon described worldwide by many workers (e.g., Hutton 1982; Hibbard 1987; Vernon *et al.* 2004), results when induced strain rate exceeds the rate of magma escape through filter pressing (Dell'Angelo and Tullis 1988; Rutter and Neumann 1995; Park and Means 1996). The transgranular fractures without fracture infills are punctured and cross-cut both phenocrysts and groundmass and are interpreted to have occurred after the completion of the crystallisation of the BG magma. Based on the microstructural observations, we conclude that the Bundelkhand magma cooled slowly with a prevailing magmatic to sub-magmatic flow. During the magmatic to sub-magmatic flow, the mush of early formed phenocrysts were strained due to the mutual interaction along their grain boundaries while the groundmass, representing the molten portion in the interstitial spaces formed by the crystal mush, deformed by viscous flow and escaped any straining, related to solid-state deformation (Paterson *et al.* 1989; Vernon 2000; Sarkar *et al.* 2017).

6. Conclusions

At the initial stage, the crystal mush is deformed by the dislocation of creep- and melt-assisted diffusion creep, and at the later stage, by fracturing with contemporaneous melt percolation. The deformation by fracturing continued after the solidification as evidenced by the presence of unhealed fractures affecting all earlier structures. The switching of deformation mechanisms from dislocation and melt-assisted diffusion creep to brittle fracturing during the magmatic to the sub-magmatic flow possibly linked to a complex relationship between the induced strain rate and the progressive rise of melt viscosity as a result of cooling. To summarise, based on the evidences presented in this work, it is undeniable that amidst the entire course of magmatic to sub-magmatic condition, the deformation is strongly decoupled between the early formed crystals/crystal mush and surrounding melts (Dell'Angelo and Tullis 1988; Rutter and Neumann 1995). The exact causes of the transformation of deformation mechanisms are, however, still elusive and need further research. It is also unclear whether the latter fractures affecting all earlier structures represent a different deformation episode or the same deformation phase that continued from the sub-magmatic to solid-state condition and thus, require further investigations.

Acknowledgements

This study is a part of the doctoral research of GS. The authors sincerely thank the EMPA laboratory

members of Banaras Hindu University, especially, Prof N V Chalapathi Rao and Dr Dinesh Pandit for the EPMA analysis. The authors also acknowledge the infrastructural facilities provided by Banaras Hindu University. The authors are grateful to two anonymous reviewers for their comments and the handling editor Prof Saibal Gupta for his suggestions that improved the quality of the article. SB acknowledges the financial help provided by DST SERB under project ECR/2018/000586. This study marks the first contribution of the Laboratory for Analyses of Magnetic and Petrofabric (LAMP) at Banaras Hindu University.

References

Barros C E M, Barbey P and Boullier A M 2001 Role of magma pressure, tectonic stress and crystallization progress in the emplacement of syntectonic granites. The A-type Estrela granite complex (Carajás Mineral Province, Brazil). *Tectonophys.* **343**(**1–2**) 93–109.

Basu A 1986 Geology of parts of the Bundelkhand granite massif central India; Record, Geol. Surv. India, 117p.

Basu A 2007 Role of the Bundelkhand Granite Massif and the Son–Narmada megafault in Precambrian crustal evolution and tectonism in Central and Western India; *J. Geol. Soc. India* **70**(**5**) 745–770.

Bhattacharya A R and Singh S P 2013 Proterozoic crustal scale shearing in the Bundelkhand massif with special reference to quartz reefs; *J. Geol. Soc. India* **82**(**5**) 474–484.

Bouchez J L, Delas C, Gleizes G, Nedelec A and Cuney M 1992 Submagmatic microfractures in granites; *Geology* **20**(**1**) 35–38.

Dell'Angelo L N and Tullis J 1988 Experimental deformation of partially melted granitic aggregates; *J. Metamorph. Geol.* **6**(**4**) 495–515.

Dell'Angelo L N, Tullis J and Yund R A 1987 Transition from dislocation creep to melt-enhanced diffusion creep in fine-grained granitic aggregates; *Tectonophys.* **139**(**3–4**) 325–332.

Fernández C and Castro A 1999 Brittle behaviour of granitic magma: The example of Puente del Congosto, Iberian Massif, Spain; *J. Geol. Soc. London, Spec. Publ.* **168**(**1**) 191–206.

Hibbard M J 1987 Deformation of incompletely crystallized magma systems: Granitic gneisses and their tectonic implications; *J. Geol.* **95**(**4**) 543–561.

Hutton D H W 1982 A tectonic model for the emplacement of the Main Donegal granite, NW Ireland; *J. Geol. Soc. London* **139**(**5**) 615–631.

Kaur P, Zeh A, Chaudhri N and Eliyas N 2016 Unravelling the record of Archaean crustal evolution of the Bundelkhand Craton, northern India using U–Pb zircon–monazite ages, Lu–Hf isotope systematics, and whole-rock geochemistry of granitoids; *Precamb. Res.* **281** 384–413.

Mohan M R, Singh S P, Santosh M, Siddiqui M A and Balaram V 2012 TTG suite from the Bundelkhand Craton, Central India: Geochemistry, petrogenesis and implications for Archean crustal evolution; *J. Asian Earth Sci.* **58** 38–50.

Mondal M E A and Zainuddin S M 1996 Evolution of the Archean–Palaeoproterozoic Bundelkhand Massif, central India – evidence from granitoid geochemistry; *Terra Nova* **8**(**6**) 532–539.

Mondal M E A, Goswami J N, Deomurari M P and Sharma K K 2002 Ion microprobe $^{207}Pb/^{206}Pb$ ages of zircons from the Bundelkhand massif, northern India: Implications for crustal evolution of the Bundelkhand–Aravalli protocontinent; *Precamb. Res.* **117**(**1–2**) 85–100.

Park Y and Means W D 1996 Direct observation of deformation processes in crystal mushes; *J. Struct. Geol.* **18**(**6**) 847–858.

Paterson S R, Vernon R H and Tobisch O T 1989 A review of criteria for the identification of magmatic and tectonic foliations in granitoids; *J. Struct. Geol.* **11**(**3**) 349–363.

Pati J K, Patel S C, Pruseth K L, Malviya V P, Arima M, Raju S, Pati P and Prakash K 2008 Geology and geochemistry of giant quartz veins from the Bundelkhand Craton, central India and their implications; *J. Earth Syst. Sci.* **116**(**6**) 497.

Rahman A and Zainuddin S M 1993 Bundelkhand granites: An example of collision-related Precambrian magmatism and its relevance to the evolution of the central Indian shield; *J. Geol.* **101**(**3**) 413–419.

Rutter E H and Neumann D H K 1995 Experimental deformation of partially molten Westerly granite under fluid-absent conditions, with implications for the extraction of granitic magmas; *J. Geophys. Res.* **100**(**B8**) 15,697–15,715.

Saha L, Pant N C, Pati J K, Upadhyay D, Berndt J, Bhattacharya A and Satynarayanan M 2011 Neoarchean high-pressure margarite–phengitic muscovite–chlorite corona mantled corundum in quartz-free high-Mg, Al phlogopite–chlorite schists from the Bundelkhand craton, north central India; *Contrib. Mineral. Petrol.* **161**(**4**) 511–530.

Sarkar G, Matin A and Sensarma S 2017 Submagmatic fabric in the 2.6 Ga Bundelkhand granitoid, India: Evidence from microstructure; *Curr. Sci.* **112**(**2**) 348–354.

Sensarma S, Matin A, Paul D, Patra A, Madhesiya A K and Sarkar G 2018 Reddening of ∼2.5 Ga granitoid by high-temperature fluid linked to mafic dyke swarm in the Bundelkhand Craton, north central India; *Geol. J.* **53**(**4**) 1338–1353.

Vernon R H 2000 Review of microstructural evidence of magmatic and solid-state flow; *Vis. Geosci.* **5**(**2**) 1–23.

Vernon R H, Johnson S E and Melis E A 2004 Emplacement-related microstructures in the margin of a deformed pluton: The San José tonalite, Baja California, México; *J. Struct. Geol.* **26**(**10**) 1867–1884.

Vigneresse J L and Tikoff B 1999 Strain partitioning during partial melting and crystallizing felsic magmas; *Tectonophys.* **312** 117–132.

Corresponding editor: Saibal Gupta